The Journal of Pathology: Clinical Research
J Pathol Clin Res November 2021; **7:** 590–603
Published online 2 July 2021 in Wiley Online Library (wileyonlinelibrary.com). DOI: 10.1002/cjp2.232

ORIGINAL ARTICLE

Integration of NRP1, RGS5, and FOXM1 expression, and tumour necrosis, as a postoperative prognostic classifier based on molecular subtypes of clear cell renal cell carcinoma

Takashi Yoshida[1]*, Chisato Ohe[2], Junichi Ikeda[2], Naho Atsumi[2], Ryoichi Saito[1], Hisanori Taniguchi[1], Haruyuki Ohsugi[1], Motohiko Sugi[1], Koji Tsuta[2], Tadashi Matsuda[1] and Hidefumi Kinoshita[1]

[1]*Department of Urology and Andrology, Kansai Medical University, Hirakata, Japan*
[2]*Department of Pathology and Laboratory Medicine, Kansai Medical University, Hirakata, Japan*

**Correspondence to: Takashi Yoshida, Department of Urology and Andrology, Kansai Medical University, 2-3-1 Shin-machi, Hirakata, Osaka 573-1191, Japan. E-mail: yoshidtk@takii.kmu.ac.jp*

Abstract

Molecular mechanisms of progression of clear cell renal cell carcinoma (ccRCC) have been proven with recent genomic or transcriptional analyses. However, it is still difficult to apply these analyses to daily clinical practice owing to economical and practical issues. Here, we established a pathology-based, postoperative prognostic classification based on the well-validated transcriptional classifier, ClearCode34, in ccRCC. A total of 342 cases with available tissue were identified and randomly allocated into a discovery cohort ($n = 138$) and a validation cohort ($n = 204$). Levels of mRNA were quantified using a nCounter Digital Analyzer, and the ccA/ccB subtypes were determined. Histological and immunohistochemistry (IHC) analyses were subsequently performed to establish a pathology-based classification based on the mRNA levels. Finally, the prognostic ability of the new classifier was evaluated in both the discovery and validation cohorts. Of 138 cases in the discovery cohort, 78 (56.5%) and 60 (43.5%) were assigned to the ccA and ccB subtypes, respectively. Proangiogenic genes, neuropilin 1 (*NRP1*) and regulator of G protein signalling 5 (*RGS5*), were especially overexpressed in all ccRCC samples and were enriched in ccA-assigned tumours. Histologically, tumour necrosis and the sarcomatoid feature were associated with the ccB subtype. In IHC analyses, expression of NRP1, RGS5, and forkhead box M1 (FOXM1), an epithelial–mesenchymal transition-related factor, significantly correlated with the ccA/ccB subtypes. Combining these three IHC factors and tumour necrosis, we developed the IHC/histology-based classifier, which showed good concordance with the ClearCode34 classifier with an accuracy of 0.80. The established classification significantly stratified relapse-free, cancer-specific, and overall survival rates in both the discovery and validation cohorts. The novel molecular pathology classifier integrating NRP1, RGS5, FOXM1, and tumour necrosis may enable the stratification of oncological outcomes for patients with ccRCC undergoing resection surgery.

Keywords: clear cell renal cell carcinoma; histology; immunohistochemistry; molecular subtype; prognostic classification

Received 29 January 2021; Revised 16 May 2021; Accepted 2 June 2021

No conflicts of interest were declared.

Introduction

Clear cell renal cell carcinoma (ccRCC) is the most prevalent histological subtype of kidney cancer, accounting for approximately 75% of RCCs [1]. Over 90% of ccRCCs are characterised by inactivating mutations in the von Hippel–Lindau (*VHL*) gene. This gene encodes the VHL protein that targets the transcription factors, hypoxia-inducible factors (HIFs), for proteasomal degradation [2,3]. HIFs are stabilised/activated in response to hypoxic stress, and they trigger new blood vessel formation by activating the vascular endothelial growth factor (VEGF) [4,5]. Accordingly, anti-VEGF drugs, such as tyrosine kinase inhibitors (TKIs), have been the mainstay of therapy for metastatic RCC (mRCC) in the last two decades. However, their efficacy is relatively limited for such patients [6], which has led to the exploration of pathways related to resistance to TKIs and to the search for novel target markers.

Several molecular classifications based on genomic, transcriptomic, and metabolomic analyses have been established, and their association with clinical outcomes has been shown for RCC [7]. In the current clinical setting, however, molecular-based analyses remain challenging and prohibitive for many medical institutions owing to economic and practical issues [8,9]. Extensive efforts have been made to identify pathology-based surrogates for molecular classification that can be adopted for daily practical use in several 7malignancies [9–11], but there have been few studies on the development of immunohistochemistry (IHC)-based surrogate classification in ccRCC. This is probably because of the greater difficulty in predicting transcript levels compared to protein levels, with a concordance rate of only 32% ($r = 0.23$) [12,13]. Hence, in the present study, we aimed to establish an IHC/histology-based classifier based on the most well-validated molecular classification of ccRCC namely ClearCode34 [14–18]. This transcriptional classification consists of genes related to several mechanisms, including hypoxia, angiogenesis, fatty/organic acid metabolism, epithelial–mesenchymal transition (EMT), cell cycle, and wound healing, and facilitates predictions for postoperative relapse of localised/advanced ccRCC [14–18]. First, because of the lack of its external validation in the Asian population, we assessed the reproducibility of the ClearCode34 classifier in our cohort, with respect to the prognostic value and tumour heterogeneity [14–18]. Subsequently, histological and IHC analyses were performed to identify minimal markers corresponding to molecular subtypes for the development of the pathology-based prognostic classifier (Figure 1).

Materials and methods

Ethics and selection of cases

The present study was approved by the institutional review board of Kansai Medical University (No. 2018109). In this study, we included 342 ccRCC patients undergoing resection surgery, whose formalin-fixed, paraffin-embedded (FFPE) tissues from the primary lesion were available. These patients underwent surgery, such as radical or partial nephrectomy, between January 2006 and June 2017 at Kansai Medical University Hospital. No synchronous or metachronous bilateral tumours, pre-surgical therapy with TKIs, or operation-related deaths were observed in these patients.

Samples and histological review

As reported previously [19], slides of whole tissue sections stained with haematoxylin and eosin were re-evaluated by a single urological surgical pathologist (CO), who was blinded to the clinical outcomes. Morphological diagnosis of ccRCC with IHC testing revealed: (1) the presence of carbonic anhydrase IX (see supplementary material, Figure S1A) and cytokeratin 7 – excluding clear cell papillary RCC [20]; (2) histological features including the World Health Organization/International Society of Urological Pathology (WHO/ISUP) grade, segmental and main renal vein invasion (RVI), sarcomatoid/rhabdoid component, and tumour-associated necrosis (the WHO Classification [21]); and (3) the pathological stage (the UICC/AJCC eighth edition TNM staging system [22]). For primary tumour lesions, we prepared two tissue microarray (TMA) cores ($\Phi = 2$ mm) for each case, which we obtained from the FFPE tissue block(s) that had been carefully selected from the most representative area (i.e. the highest grade [15,17]). Moreover, we sampled FFPE tissue blocks from the RVI tumour, and the relapsed tumour was resected by metastasectomy for molecular subtyping, if these were available (see supplementary material, Figure S1B).

RNA isolation and gene expression analysis

Total RNA was isolated from 1-mm cores of tumour-rich areas of FFPE tissue blocks, which were selected from the most representative location, as described above, by homogenisation of each sample using the ReliaPrep™ FFPE Total RNA Miniprep System (Promega, Madison, WI, USA). Levels of mRNA were assessed for a custom gene panel, which included the 34 genes in ClearCode34, as reported previously [15]. Gene expression was quantified using an nCounter Digital Analyzer (NanoString Technologies Inc., Seattle, WA, USA), and raw counts were generated using nSolver™ 4.0 Analysis Software (NanoString Technologies Inc.). The NanoString data were corrected using positive and negative spike-in controls and were normalised using five reference genes (*C14orf166*, *RPLR1*, *SNRPD2*, *TBP*, and *ABCF1*). To classify the ccA/ccB subtypes, unsupervised hierarchical clustering (median clustering and correlation distance) was performed using *hclust* in R for the NanoString data for the combined primary, RVI, and relapsed tumour samples [17].

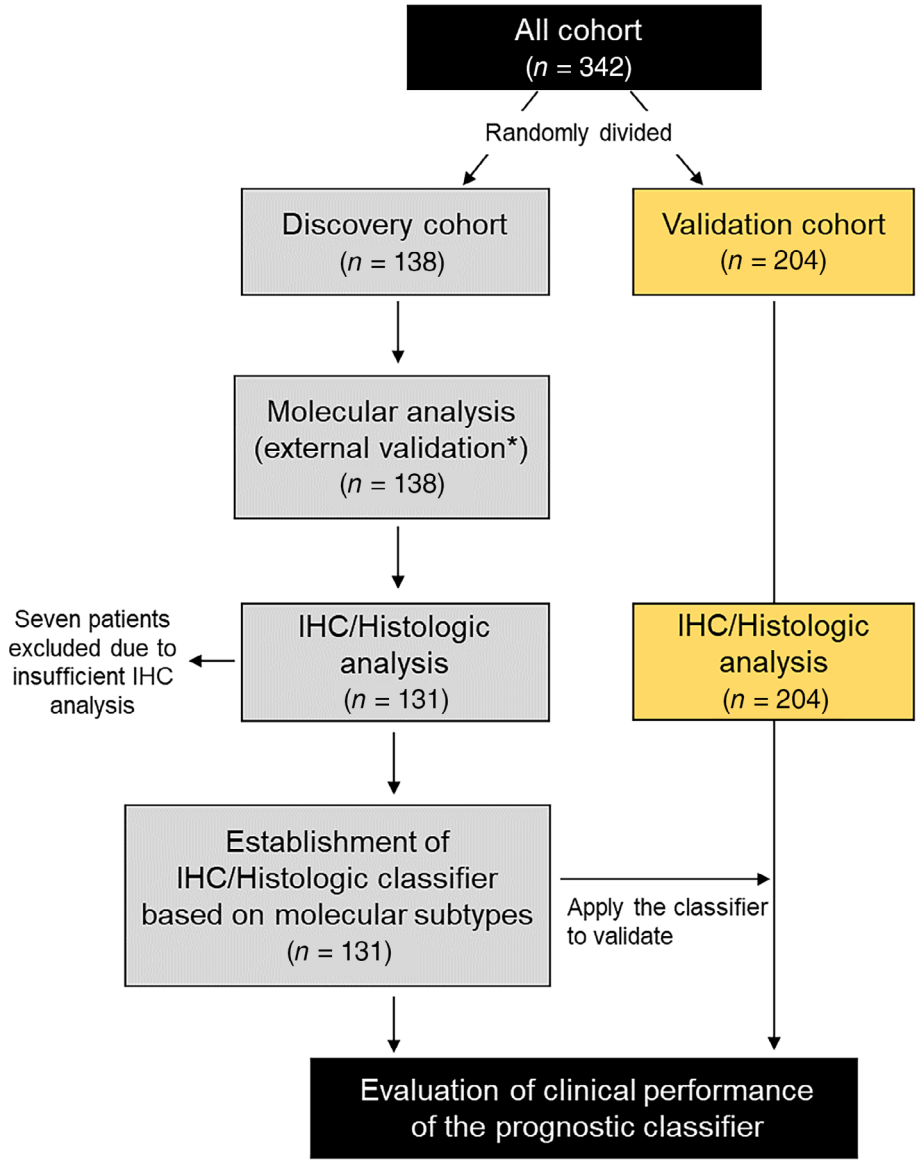

Figure 1. Workflow for the discovery of IHC/histology-based prognostic classification based on molecular subtypes: *ClearCode34 [14], which was applied for external validation.

Immunohistochemical analysis

Sections cut at 4 μm from the FFPE-TMA blocks were deparaffinised and rehydrated with xylene and alcohol solutions. IHC staining was performed on two cores per case using Leica Bond-III (Leica Biosystems, Melbourne, Australia) and visualised using BOND Polymer Refine Detection (Leica Biosystems). To find minimal markers as IHC surrogates for clinical use, candidate IHC antibodies were selected based on the algorithm described in supplementary material, Figure S2. Neuropilin 1 (NRP1), regulator of G protein signalling 5 (RGS5), forkhead box M1 (FOXM1), receptor tyrosine kinase-like orphan receptor 2 (ROR2), and polypeptide *N*-acetylgalactosaminyltransferase10 (GALNT10) were finally used as primary antibodies (see supplementary material, Table S1). Protein expression seen using IHC was evaluated semi-quantitatively by two independent pathologists – CO for the discovery cohort and JI for the validation cohort – using the H-score = the staining intensity (0 = none; 1 = weak; 2 = moderate; 3 = strong) × the percentage of

positive cells [23]. The H-score of each case was determined as a mean value of H-scores of the two cores.

Statistical analyses

A chi-squared test, Fisher's exact test, and Student's *t*-test were used to evaluate the statistical significance between the two variables. For intratumour heterogeneity (primary versus RVI tumour) and longitudinal heterogeneity (primary/RVI tumour versus relapsed tumour), 95% confidence intervals (CIs) were calculated using the exact method [17]. Relapse-free survival (RFS; relapse was defined as the time from surgery to initial local or distant relapse on imaging), cancer-specific survival (CSS), and overall survival (OS) were assessed using the Kaplan–Meier method with the log-rank test and the Cox proportional hazards model. The associations of pathological factors were analysed using the logistic regression model. A receiver-operating characteristic (ROC) curve was used to quantify the area under the curve (AUC) and determine the cut-off value. All statistical analyses were performed using EZR version 1.51 (https://www.jichi.ac.jp/saitama-sct/SaitamaHP.files/statmedEN.htm) [24]. A two-sided $p < 0.05$ was considered statistically significant.

Results

Patients and pathological characteristics

The clinicopathological findings of all patients are presented in Table 1. The population was randomly divided into two cohorts (2:3): the discovery cohort, 138 patients (40.4%); the validation cohort, 204 patients (59.6%). The discovery cohort had worse pathological staging and the presence of RVI compared to the validation cohort (all, $p < 0.001$). The WHO/ISUP grade, sarcomatoid/rhabdoid features, and tumour necrosis were equivalent between the two cohorts. In the discovery cohort, 40 (87.0%) of 46 cases with concomitant RVI, and 9 (25.0%) of 36 cases, who experienced postoperative relapse, were successfully analysed with the NanoString molecular analysis.

Table 1. Clinicopathological characteristics of 342 patients.

Variables	Discovery cohort ($n = 138$)	Validation cohort ($n = 204$)	*P* value
Age at surgery, years, median, (IQR)	63.5 (38.0–85.0)	66.0 (57.0–73.3)	0.160
Gender, *n* (%)			
Female	37 (26.8)	62 (30.4)	0.544
Male	101 (73.2)	142 (69.6)	
Pathological staging (TNM2018), *n* (%)			
I	71 (51.4)	153 (75.0)	<0.001
II	6 (4.3)	7 (3.4)	
III	52 (37.7)	26 (12.7)	
IV	9 (6.5)	18 (8.8)	
WHO/ISUP grade, *n* (%)			0.352
1	13 (9.4)	32 (15.7)	
2	72 (52.2)	99 (48.5)	
3	38 (27.5)	56 (27.5)	
4	15 (10.9)	17 (8.3)	
Sarcomatoid/rhabdoid features, *n* (%)			0.195
Absent	125 (90.6)	193 (94.6)	
Present	13 (9.4)	11 (5.4)	
RVI*, *n* (%)			<0.001
Absent	87 (65.4)	186 (91.2)	
Present	46 (34.6)	15 (7.4)	
Missing	5 (3.6)	3 (1.5)	
Tumour necrosis, *n* (%)			1.000
Absent	108 (78.3)	160 (78.4)	
Present	30 (21.7)	44 (21.6)	
Relapse, *n* (%)	36 (26.1)	35 (17.2)	0.057
Cancer-specific mortality, *n* (%)	14 (10.1)	14 (6.9)	0.317
Overall mortality, *n* (%)	27 (19.6)	30 (14.7)	0.241

IQR, interquartile range.
*Segmental and main RVIs.

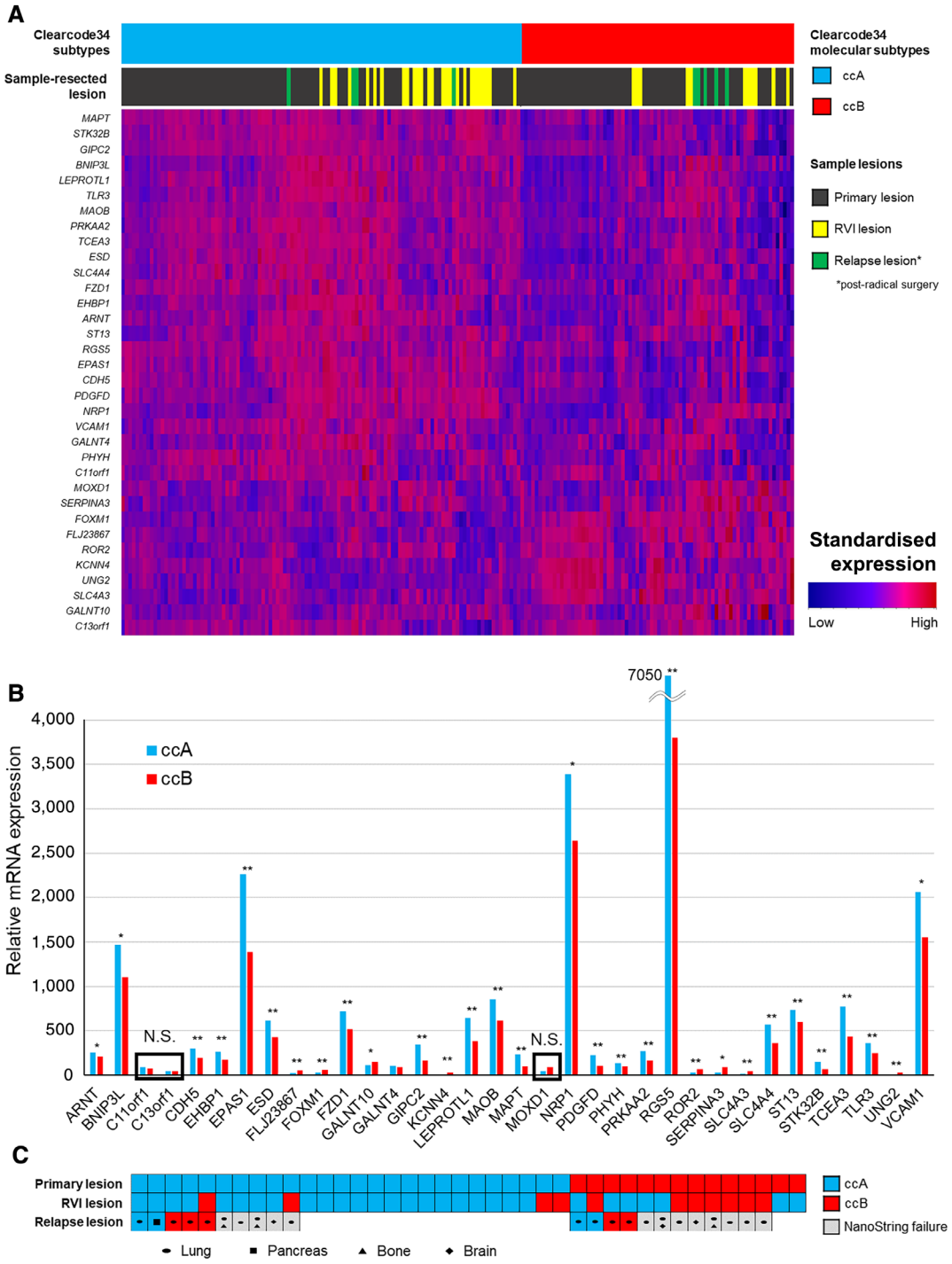

Figure 2. (A) Heatmap displaying hierarchical clustering analysis of the ClearCode34 gene profiles in the discovery cohort. The colour bar on the top of the heatmap represents clear cell type A (ccA) and B (ccB) subtypes (blue indicates ccA and red indicates ccB). The second tier of the colour bar represents sample-resected lesions (black indicates primary lesion, yellow indicates RVI lesion, and green indicates postoperative relapse lesion). (B) Distribution and comparison of relative mRNA levels of all 34 genes between ccA and ccB subtypes. Statistical analysis using Student's *t*-test $*p < 0.01$, $**p < 0.001$; N.S., not significant. (C) The molecular subtype of patient-matched primary and RVI tumour lesions for 40 ccRCC patients. A blue box indicates that the tumour was classified as ccA, a red box indicates that the tumour was classified as ccB, and a grey box indicates that the tumour was not successfully evaluated by the NanoString assay.

ccA/ccB molecular subtyping

Using an established 34-gene classifier set, hierarchical clustering was performed to assess external validity in our Japanese patients; two clusters were identified in the discovery cohort (Figure 2A). Of all 187 samples, 111 (59.4%; primary tumour: $n = 78$, RVI tumour: $n = 29$, and relapsed tumour: $n = 4$) were assigned to the ccA subtype, and 76 (40.6%; primary tumour: $n = 60$, RVI tumour: $n = 11$, relapsed tumour: $n = 5$) were assigned to the ccB subtype. Preoperative clinical factors (e.g. age, gender, and clinical TNM staging) and surgical types were well balanced between the two subtype groups (see supplementary material, Table S2). The relative mRNA levels of all 34 genes, except *MOXD1*, *C11orf1*, and *C13orf1*, differed significantly between the subtypes (Figure 2B), with levels of *RGS5* and *NRP1* being extremely high in all ccRCC tissue samples.

In 40 patients, intratumour heterogeneity was accessed by identifying the ccA/ccB molecular subtypes of patient-matched primary and RVI tumours. Only 11 (27.5%, 95% CI 1.0–32.6%) of 40 patients had heterogeneous tumours (Figure 2C). We then longitudinally assessed the discordance of molecular subtypes between the primary or RVI tumours and relapsed tumours in the same patients. Of nine cases, discordance was observed between relapsed tumours and five primary tumours (55.5%, 95% CI 0.03–18.2%) as well as five RVI tumours (55.5%, 95% CI 0.01–78.3%) (Figure 2C).

Prognostic significance of ccA/ccB molecular subtypes

Survival curve analysis showed that the 5-year RFS rate was significantly lower in patients with the ccB subtype than in those with the ccA subtype (65.1 versus 86.2%, $p = 0.001$; Figure 3A). In addition, the 5-year CSS rate was significantly lower in patients with the ccB subtype than in those with the ccA subtype (87.5 versus 96.9%, $p = 0.034$; Figure 3B).

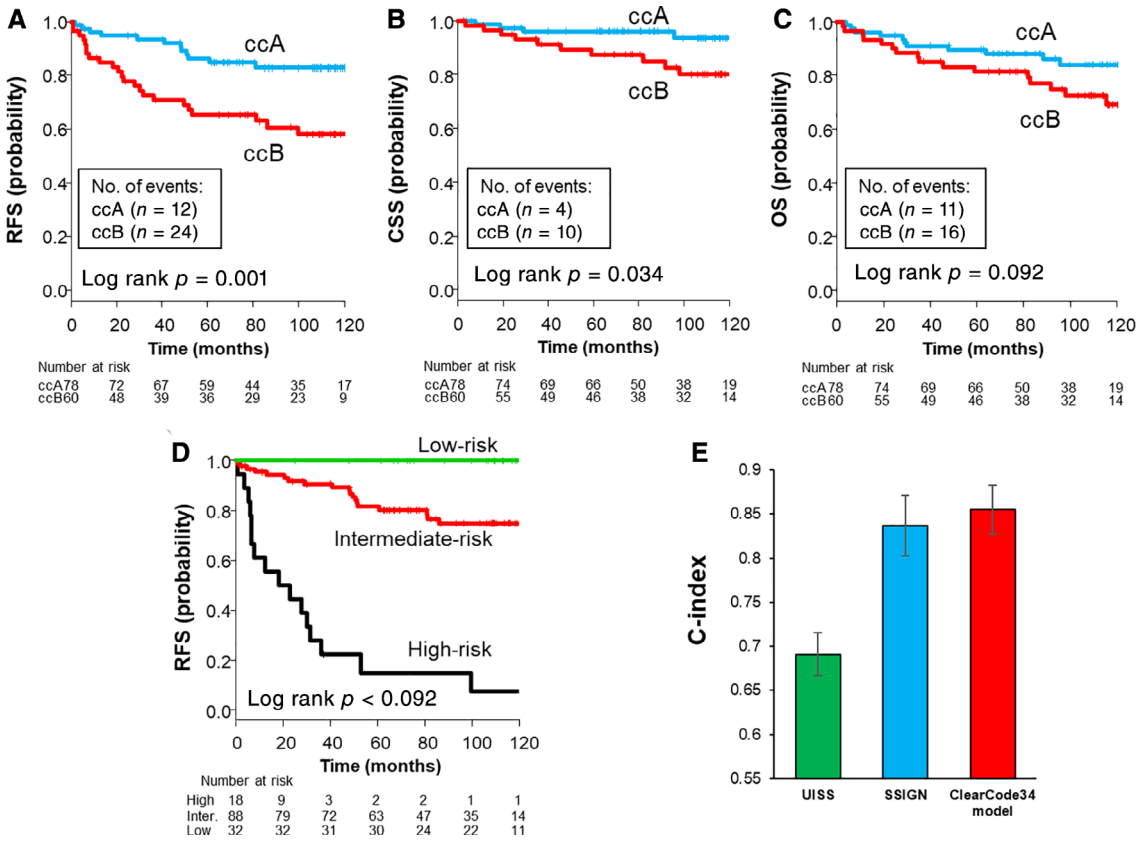

Figure 3. Kaplan–Meier curves stratified by ClearCode34 molecular subtypes (ccA/ccB): (A) RFS, (B) CSS, and (C) OS. (D) Kaplan–Meier curve of RFS stratified by the ClearCode34 model reported by Brooks *et al* (ccA/ccB subtypes, tumour stage, and histological grade) [15]; *P* values were calculated using the log-rank test. (E) Concordance indices of the three risk models, including Mayo Clinic Stage, Size, Grade, and Necrosis (SSIGN); ClearCode34 model; and the UISS, to predict the risk of postoperative relapse.

However, there was no significant difference in OS between the two subtypes (Figure 3C).

Based on a relapse-prediction model (ClearCode34 model), proposed by Brooks *et al* [15], which incorporates subtypes, grade, and staging, we generated the multivariate regression model integrating the ccA/ccB subtypes ($p = 0.036$), TNM staging ($p < 0.001$), and tumour grade ($p < 0.001$) using our cohort (see supplementary material, Table S3). The survival curve of RFS was significantly stratified by the model ($p < 0.001$; Figure 3D). The prognostic accuracy of ClearCode34 was superior to that of the Mayo Clinic Stage, Size, Grade, and Necrosis (SSIGN) score (c-index 0.855 versus 0.837) [25] and the University of California, Los Angeles (UCLA) Integrated Staging System (UISS) (c-index 0.855 versus 0.691) [26] (Figure 3E).

Histological and IHC evaluation of ccA/ccB molecular subtypes

Logistic regression analysis demonstrated that the presence of sarcomatoid/rhabdoid features (odds ratio [OR] 8.53, $p < 0.001$) and tumour necrosis (OR 5.07, $p < 0.001$) significantly correlated with the ccB subtype (Figure 4A). Specifically, 73% (22/30) of cases with tumour necrosis and 77.8% (7/9) of cases with sarcomatoid features were enriched in the ccB subtype

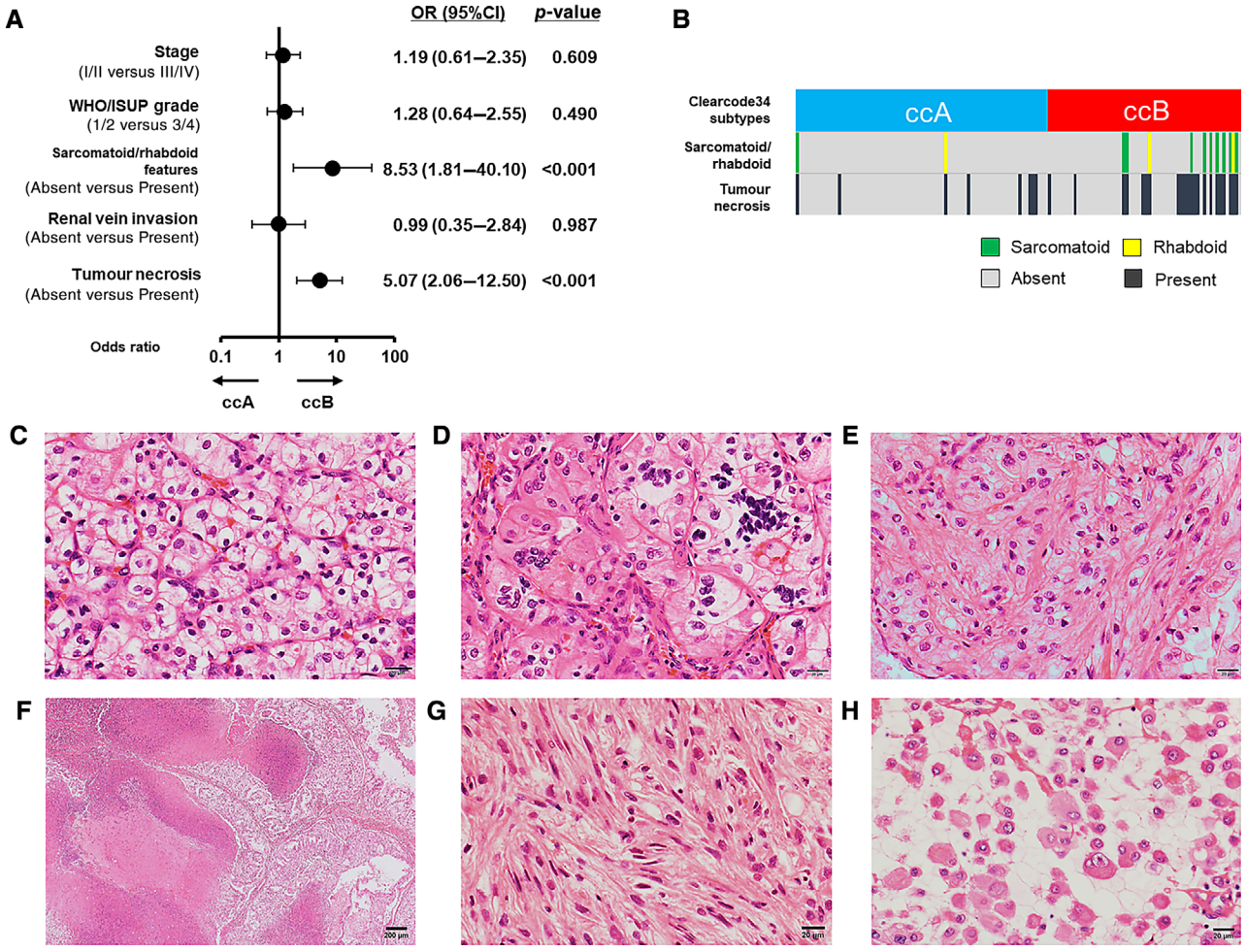

Figure 4. (A) Forest plot showing the ORs and 95% CI of pathological factors for predicting the ccA/ccB subtypes. Logistic regression analysis was used for statistical analysis. (B) Distribution of sarcomatoid/rhabdoid features and tumour-associated necrosis in the ccA/ccB subtypes. Representative haematoxylin and eosin stains stratified by (C,D) ccA and (E–H) ccB; (C) tumour cells with clear cytoplasm surrounded by distinct cell membranes and small thin-walled vasculature and (D) tumour cells with both clear and eosinophilic cytoplasm surrounded by vasculature. Two of three cases with multinucleated giant cells were assigned to ccA, (E) eosinophilic ccRCC without surrounding vasculature network, (F) the presence of tumour-associated necrosis around the tumour, (G) sarcomatoid features, and (H) rhabdoid features.

(Figure 4B and supplementary material, Table S4). Representative histological findings are displayed in Figure 4C–E; tumours assigned to the ccA subtype often showed typical morphology such as glycogen content (± concomitant eosinophilic cytoplasm) with a network of tumour blood vessels (Figure 4C,D). In addition to the typical morphology, tumour with eosinophilic features (Figure 4E), tumour necrosis (Figure 4F), sarcomatoid (Figure 4G), and rhabdoid features (Figure 4H) were observed in the ccB-assigned tumours.

Antibodies against NRP1, RGS5, FOXM1, ROR2, and GALNT10 were selected for IHC analysis (see supplementary material, Figure S2) [27–31]. Of 138 cases, IHC was performed successfully for 131 (94.9%) cases in the discovery cohort. As shown in Figure 5 with representative figures of these markers, we confirmed that NRP1 and RGS5 expression were significantly greater in cases of the ccA subtype than in those of the ccB subtype ($p = 0.001$ and $p < 0.001$, respectively). In contrast, although FOXM1 overexpression was confirmed in ccB cases ($p < 0.001$), there was no difference in ROR2 or GALNT10 expression between the subtypes.

Development of an IHC/histology-based classifier corresponding to ccA/ccB molecular subtypes

To facilitate the use of IHC parameters, the cut-off values of NRP1, RGS5, and FOXM1 levels were determined using ROC analyses (Figure 6A).

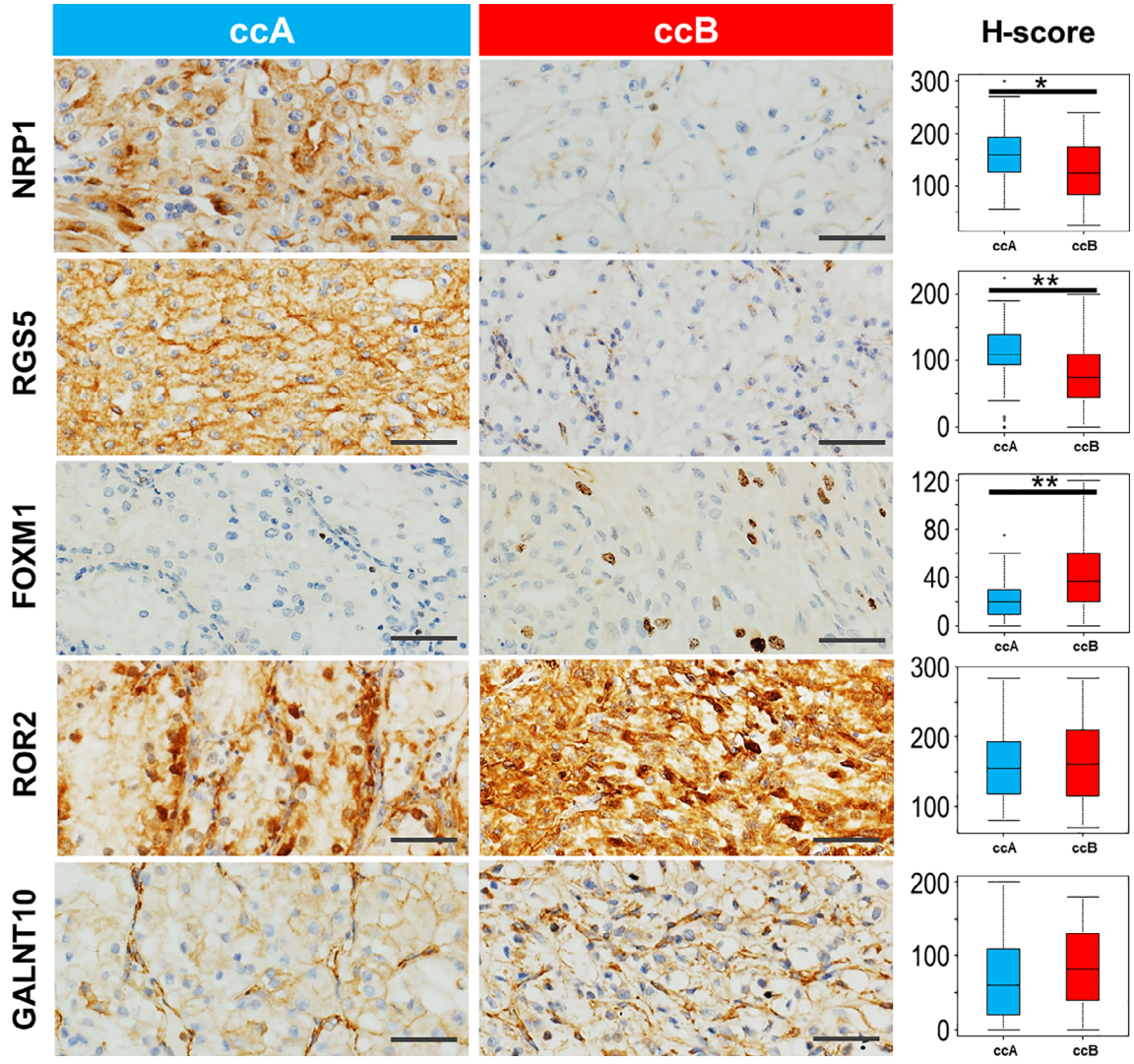

Figure 5. Representative immunostains and H-scores for NRP1, RGS5, FOXM1, ROR2, and polypeptide GALNT10 expression. The antibodies used and evaluation site for each stain are described in supplementary material, Table S1. Statistical analysis using Student's *t*-test $^{*}p < 0.01$, $^{**}p < 0.001$. Scale bars: 40 μm.

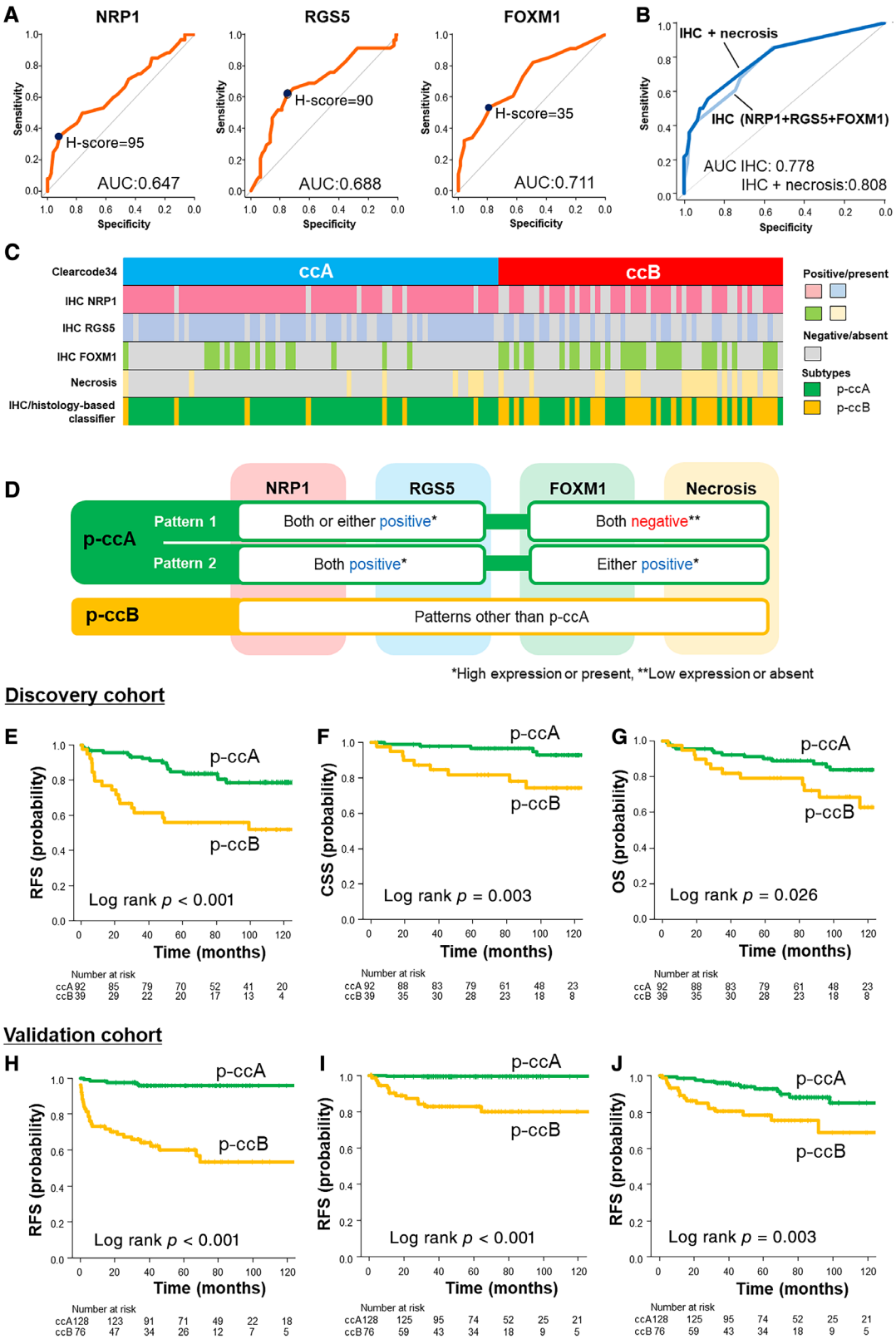

Figure 6. Legend on next page.

Table 2. Multivariate analysis of IHC/histological factors associated with ClearCode34 molecular subtypes in the discovery cohort.

Models	OR	95% CI	*P* value	AUC
IHC only				
NRP1 (high versus low)	0.211	0.07–0.64	0.006	0.778
RGS5 (high versus low)	0.227	0.10–0.54	<0.001	
FOXM1 (high versus low)	5.010	2.12–11.80	<0.001	
Histological features + IHC (final model)				
Sarcomatoid features* (present versus absent)	–	–	–	
Tumour necrosis (present versus absent)	4.030	1.41–11.50	0.009	0.808
NRP1 (high versus low)	0.237	0.08–0.72	0.011	
RGS5 (high versus low)	0.237	0.10–0.59	0.002	
FOXM1 (high versus low)	4.840	1.95–12.00	<0.001	

*Sarcomatoid change was excluded after stepwise selection.

Multivariate logistic regression analyses revealed that the three markers (dichotomised by the cut-off values) were independently associated with the ccA/ccB molecular classifier, even after adjusting histological features such as tumour necrosis and the sarcomatoid feature (Table 2). The sarcomatoid feature was eliminated by using the backward stepwise procedure. The AUC of the IHC-based model was improved from 0.778 to 0.808 by adding a histological factor – tumour necrosis (Figure 6B). When applying the cut-off of 0.70 (Youden index) – the propensity score calculated from the logistic regression model – two distinct pathology-based subtypes were obtained (pathologic-ccA [p-ccA]: $n = 92$, and p-ccB: $n = 39$), which had good statistical concordance with RNA-based ccA/ccB subtypes (chi-squared test: $p < 0.001$; Figure 6C). A proposed IHC/histology-based classifier based on ClearCode34 is described in Figure 6D.

Verification and validation of the IHC/histology-based classifier for oncological outcomes

The prognostic ability of the developed classifier was assessed in the discovery cohort. Survival curve analysis showed that the 5-year RFS rate was significantly lower in patients with the p-ccB subtype than in those with p-ccA (65.1 versus 86.2%, $p < 0.001$; Figure 6E). Moreover, the 5-year CSS and OS rates were significantly lower in patients with the p-ccB subtype than in those with p-ccA (CSS: 81.5 versus 96.5%, $p = 0.003$; OS: 79.1 versus 90.0%, $p = 0.026$; Figure 6F,G). Compared to the ccA/ccB molecular subtypes, our IHC/histology-based classifier showed substantially improved prognostic accuracy for RFS (0.63 versus 0.65) and CSS (0.63 versus 0.70; see supplementary material, Figure S3).

The Cancer Genome Atlas (TCGA) report from 2018 [2] reported that *TP53* and breast cancer type 1-associated protein 1 (*BAP1*) mutations were correlated to poor outcomes; therefore, we compared the prognostic significance of the IHC/histology-based classifier with that of these IHC markers. The reliability of p53 and BAP1 IHC-based assays for detecting mutations in these genes has been established previously [32,33]. Both p53 and BAP1 negativity was significantly correlated with decreased RFS rate, but neither marker was correlated with poor CSS rate (see supplementary material, Figure S4A,B). Regarding prognostic accuracy, the IHC/histology-based classifier showed a higher concordance index (c-index) than these two markers with respect to RFS and CSS (see supplementary material, Figure S4C).

Finally, we assessed the prognostic ability of this classification using the validation cohort. After the assessment of IHC analysis using NRP1, RGS5, and FOXM1 by an independent pathologist, 204 cases

Figure 6. (A) ROC curve analyses for NRP1, RGS5, and FOXM1 expression predicting ccA/ccB subtypes. The cut-off value of the H-score for each marker was determined using the Youden index. (B) ROC curves for comparison of propensity scores calculated from logistic regression models of IHC only versus IHC + tumour necrosis (Table 2). (C) Distribution of p-ccA/ccB subtypes based on the IHC/histology-based classifier and ClearCode34 molecular subtypes. Propensity scores of <0.7 and ≥0.7 were assigned to p-ccA and p-ccB subtypes, respectively. (D) A schema of the IHC/histology-based classifier. The p-ccA subtype is determined by pattern 1: NRP (+), RGS5 (+), FoxM1 (−), necrosis (−); NRP (+), RGS5 (−), FoxM1 (−), necrosis (−); or NRP (−), RGS5 (+), FoxM1 (−), necrosis (−); and pattern 2: NRP (+), RGS5 (+), FoxM1 (+) necrosis (−), or NRP (+), RGS5 (+), FoxM1 (−) necrosis (+). The p-ccB subtype has 11 patterns, which were different from the 5 patterns observed for p-ccA. Kaplan–Meier curve stratified by the IHC/histology-based classifier in the discovery and validation cohorts: (E,H) RFS, (F,I) CSS, and (G,J) OS. *P* values were calculated using the log-rank test.

were stratified into p-ccA/ccB subtypes according to the IHC/histology-based classifier: p-ccA ($n = 128$, 62.7%) and p-ccB ($n = 76$, 37.3%). In survival analyses, this classification stratified the patients' oncological outcomes between the p-ccA and p-ccB subtypes: RFS (95.9 versus 60.1%, $p < 0.001$; Figure 6H), CCS (99.2 versus 82.9%, $p < 0.001$; Figure 6I), and OS (92.6 versus 78.2%, $p = 0.003$; Figure 6J).

Discussion

The current study successfully establishes a novel pathology-based prognostic classification derived from the intrinsic molecular subtypes of ccRCC, which can be practical and cost-effective when used with daily IHC/histological analysis. Investigators have addressed ethnic/racial disparities that cause differences in RCC incidence, mortality, and histological/molecular subtypes [34,35]. In general, Asian RCC patients have favourable oncological outcomes, followed by Hispanics, whites, and blacks [34,35]. Despite this, we could identify two distinct molecular subtypes with reproducible prognostic accuracy on the basis of the 34-gene classifier, ClearCode34 (even quite low relapse rates compared to the University of North Carolina/TCGA cohorts [15]). Moreover, the present study using a Japanese cohort demonstrated that the ClearCode34 model, which consists of subtype, tumour grade, and TNM staging [15], showed higher prognostic accuracy than the conventional prognostic models (i.e. SSIGN [25] and UISS [26]) (Figure 3E), suggesting that this transcriptional classification can be a reliable prognosticator not only in white/black populations but also in Asian populations.

While previous studies investigating intratumour heterogeneity have focused on ccRCC tumours in the same area [16,17], little is known about heterogeneity between the highest grade primary lesion and the RVI tumour, which is often found with subsequent metastases and leads to poor survival rates of <60% [36]. Interestingly, 72.5% of the subtypes of RVI tissue corresponded to those of the primary tumours, which may indicate that the most malignant primary lesion extends intravenously as its invasion front. However, as previously reported [17], only half of the cases who experienced relapse had the same ccA/ccB subtypes with respect to the primary/RVI tumours and the metastatic sites. Therefore, neither the primary nor the RVI tumour would predict the nature of the lethal and therapeutically relevant metastatic tumour. Serie *et al* [17] have also addressed the high rates of intra- and inter-tumour heterogeneity within metastatic tumours, suggesting that multiple relapsed samples will be necessary if the objective is to perform a molecular-based therapeutic approach.

In the present study, to establish the new pathology-based classifier for easy use in daily practice, we focused on standard pathological factors that are routinely examined [21,22]. Sarcomatoid features were significantly enriched in the ccB subtype that overexpressed EMT-regulating genes, including *FOXM1*, *KCNN4*, *ROR2*, and *GALNT10*. This finding is consistent with previous evidence that sarcomatoid conversion is associated with a completed EMT [37], and the high expression of *FOXM1* was also linked to this result. Moreover, we found that tumour-associated necrosis was significantly higher in the ccB subtype than in the ccA subtype, which is characterised by hypoxia-related genes, *ARNT* (*HIF-β*) and *EPAS1* (*HIF-2a*). Although the precise mechanism of tumour necrosis remains unknown, this occurrence was hypothesised to be due to scarce blood supply [38]. Considering these observations, the ccB subtype seems to be shifting from its conventional nature towards the non-VHL-HIF pathway or towards the coexistence of both pathways, with a reduction in the typical vasculature network (Figure 4E,G–H). This phenomenon could be explained when looking at proangiogenic protein expression. In the present study, both protein and mRNA levels of both NRP1 (a co-receptor for VEGF [27]) and RGS5 (induced by VEGF signalling [28]) in the tumour cell were significantly lower in the ccB subtype than in the ccA subtype (Figure 5). A study by Morin *et al* [27] supports this evidence that the lack of NRP1 expression in perivascular RCC cells may have resulted in the absence of *trans*-complex formation with VEGFR2 in the tumour endothelium and therefore was associated with worse survival in RCC. However, they also suggested that this is due to increased vessel area and size, which contradicts our hypothesis. A very recent study reported by Nilsson *et al* [32] may also support our hypothesis: eosinophilic ccRCC (Figure 4E) was significantly less vascularised (CD31 and 'hallmark_angiogenesis') despite its hypoxia status ('hallmark_hypoxia'). Moreover, the gene ontology term 'hallmark_EMT' and immune cell infiltration (CD3 and CD45) were enriched in eosinophilic cells, suggesting that the eosinophilic tumour may be associated with the ccB-assigned tumour in the non-VHL-HIF pathway. To understand these findings, further translational research is required to establish objective methodology to assess vascularisation and cytoplasmic discolouration, while considering tumour heterogeneity.

In recent years, systemic therapies, including TKIs, immune checkpoint inhibitors (ICIs), or their combination, have been used for mRCC. Many studies have explored tissue-based biomarkers for predicting the response to these agents [38–43]. de Velasco *et al* found that the ccA subtype tumour is a better candidate than the ccB subtype in terms of its response to TKIs in mRCC [18]. The *PBRM1* mutation was associated with response to ICI therapy in patients who had received prior antiangiogenic therapy [39,40], whereas its presence was associated with poor response in the first-line ICI plus TKI setting [41,42]. Due to the lack of evidence regarding the association between ClearCode34 and *PBRM1* gene expression, we performed an exploratory analysis using the NanoString assay in the discovery cohort. *PBRM1* and *SETD2* were significantly downregulated in the ccB subtype compared to the ccA subtype (both, $p < 0.05$; see supplementary material, Figure S5A,C). Furthermore, some reports have suggested that sarcomatoid/rhabdoid features can be histological markers of ICI response [42,43]. In this study, the presence of sarcomatoid/rhabdoid features was significantly more marked in the ccB tumour, which was confirmed with the IHC/histology-based classifier in both the discovery and validation cohorts (see supplementary material, Table S5). Although the utility of this ccA/ccB molecular (or histological) classification in mRCC will have to be validated in clinical trials, our results suggest that the ccB molecular subtype could be a potential surrogate marker of ICI efficacy.

The present study has some limitations. First, this is a retrospective study with relatively small and heterogeneous cohorts, which may have led to a selection bias. Second, IHC analysis using TMA is not usually performed in clinical practice; hence, further evaluation using whole slides is needed. Furthermore, we used continuous values of the H-score, which is typically a categorised classification [23]. Digital image analysis may be more useful for objective IHC quantification using the H-score.

In conclusion, there is an urgent need to identify markers, involving essential molecular mechanisms that facilitate the prediction of oncological outcomes and selection of patient-matched treatment. Our IHC/histological classifier can distinguish between ccA/ccB molecular subtypes, which constitute the main ccRCC progression pathway, and is readily available in current clinical practice. For further enhancement of our classification, performing prospective, external validation with larger cohort studies and assessing predictive ability for treatment response, such as for TKI, immunotherapy, or combination therapy, will be required.

Acknowledgements

This study was supported by the Japan Society for the Promotion of Science KAKENHI fund (Grant No 20K07601 to TY, Grant No. 19K16875 to CO, Grant No. 19K18574 to HT, and Grant No. 20K16457 to HO), and the Osaka Cancer Society Foundation to CO. We thank greatly Mr Ryousuke Yamaka for his technical assistance with tissue sampling and NanoString assays.

Author contributions statement

TY and CO conceived the project. TY, CO and RS designed and performed the experiments. CO, MS and JI were responsible for tissue collection and TY and MS for the collection of clinical database information. TY wrote the manuscript. All authors reviewed and approved the final manuscript.

Data availability statement

The data that support the findings of this study are available from the corresponding author, TY, upon reasonable request.

References

1. Padala SA, Barsouk A, Thandra KC, *et al*. Epidemiology of renal cell carcinoma. *World J Oncol* 2020; **11:** 79–87.
2. Ricketts CJ, De Cubas AA, Fan H, *et al*. The Cancer Genome Atlas comprehensive molecular characterization of renal cell carcinoma. *Cell Rep* 2018; **23:** 313–326.e5.
3. Sato Y, Yoshizato T, Shiraishi Y, *et al*. Integrated molecular analysis of clear-cell renal cell carcinoma. *Nat Genet* 2013; **45:** 860–867.
4. Kaelin WG. The von Hippel-Lindau tumour suppressor protein: O2 sensing and cancer. *Nat Rev Cancer* 2008; **8:** 865–873.
5. Kondo K, Klco J, Nakamura E, *et al*. Inhibition of HIF is necessary for tumor suppression by the von Hippel-Lindau protein. *Cancer Cell* 2002; **1:** 237–246.
6. Tamaskar I, Dhillon J, Pili R. Resistance to angiogenesis inhibitors in renal cell carcinoma. *Clin Adv Hematol Oncol* 2011; **9:** 101–110.
7. Casuscelli J, Vano YA, Fridman WH, *et al*. Molecular classification of renal cell carcinoma and its implication in future clinical practice. *Kidney Cancer* 2017; **1:** 3–13.
8. Hynes SO, Pang B, James JA, *et al*. Tissue-based next generation sequencing: application in a universal healthcare system. *Br J Cancer* 2017; **116:** 553–560.

9. Tang P, Tse GM. Immunohistochemical surrogates for molecular classification of breast carcinoma: a 2015 update. *Arch Pathol Lab Med* 2016; **140:** 806–814.
10. Whitley SK, Horne WT, Kolls JK. Research techniques made simple: methodology and clinical applications of RNA sequencing. *J Invest Dermatol* 2016; **136:** e77–e82.
11. Tessier-Cloutier B, Pors J, Thompson E, *et al*. Molecular characterization of invasive and in situ squamous neoplasia of the vulva and implications for morphologic diagnosis and outcome. *Mod Pathol* 2021; **34:** 508–518.
12. Zhang B, Wang J, Wang X, *et al*. Proteogenomic characterization of human colon and rectal cancer. *Nature* 2014; **513:** 382–387.
13. Liu Y, Beyer A, Aebersold R. On the dependency of cellular protein levels on mRNA abundance. *Cell* 2016; **165:** 535–550.
14. Brannon AR, Reddy A, Seiler M, *et al*. Molecular stratification of clear cell renal cell carcinoma by consensus clustering reveals distinct subtypes and survival patterns. *Genes Cancer* 2010; **1:** 152–163.
15. Brooks SA, Brannon AR, Parker JS, *et al*. ClearCode34: a prognostic risk predictor for localized clear cell renal cell carcinoma. *Eur Urol* 2014; **66:** 77–84.
16. Gulati S, Martinez P, Joshi T, *et al*. Systematic evaluation of the prognostic impact and intratumour heterogeneity of clear cell renal cell carcinoma biomarkers. *Eur Urol* 2014; **66:** 936–948.
17. Serie DJ, Joseph RW, Cheville JC, *et al*. Clear cell type a and B molecular subtypes in metastatic clear cell renal cell carcinoma: tumor heterogeneity and aggressiveness. *Eur Urol* 2017; **71:** 979–985.
18. de Velasco G, Culhane AC, Fay AP, *et al*. Molecular subtypes improve prognostic value of International Metastatic Renal Cell Carcinoma Database Consortium prognostic model. *Oncologist* 2017; **22:** 286–292.
19. Yoshida T, Ohe C, Tsuzuki T, *et al*. Clinical impact of segmental renal vein invasion on relapse in patients with clinical T1 renal cell carcinoma undergoing partial nephrectomy. *Int J Clin Oncol* 2020; **25:** 464–471.
20. Williamson SR, Gupta NS, Eble JN, *et al*. Clear cell renal cell carcinoma with borderline features of clear cell papillary renal cell carcinoma: combined morphologic, immunohistochemical, and cytogenetic analysis. *Am J Surg Pathol* 2015; **39:** 1502–1510.
21. Moch H, Humphrey PA, Ulbright TM, *et al*. *WHO Classification of Tumours of the Urinary System and Male Genital Organs* (4th edn). IARC: Lyon, 2016.
22. Brierley JD, Gospodarowics MK, Wittekind C. *TNM Classification of Malignant Tumours*. Union for International Cancer Control (8th edn). Wiley: New York, 2017.
23. Yoshida A, Tsuta K, Wakai S, *et al*. Immunohistochemical detection of ROS1 is useful for identifying ROS1 rearrangements in lung cancers. *Mod Pathol* 2014; **27:** 711–720.
24. Kanda Y. Investigation of the freely available easy-to-use software 'EZR' for medical statistics. *Bone Marrow Transplant* 2013; **48:** 452–458.
25. Frank I, Blute ML, Cheville JC, *et al*. An outcome prediction model for patients with clear cell renal cell carcinoma treated with radical nephrectomy based on tumor stage, size, grade and necrosis: the SSIGN score. *J Urol* 2002; **168:** 2395–2400.
26. Zisman A, Pantuck AJ, Wieder J, *et al*. Risk group assessment and clinical outcome algorithm to predict the natural history of patients with surgically resected renal cell carcinoma. *J Clin Oncol* 2002; **20:** 4559–4566.
27. Morin E, Lindskog C, Johansson M, *et al*. Perivascular neuropilin-1 expression is an independent marker of improved survival in renal cell carcinoma. *J Pathol* 2020; **250:** 387–396.
28. Furuya M, Nishiyama M, Kimura S, *et al*. Expression of regulator of G protein signalling protein 5 (RGS5) in the tumour vasculature of human renal cell carcinoma. *J Pathol* 2004; **203:** 551–558.
29. Liu F, Li N, Liu Y, *et al*. Homeodomain interacting protein kinase-2 phosphorylates FOXM1 and promotes FOXM1-mediated tumor growth in renal cell carcinoma. *J Cell Biochem* 2019; **120:** 10391–10401.
30. Wright TM, Brannon AR, Gordan JD, *et al*. Ror2, a developmentally regulated kinase, promotes tumor growth potential in renal cell carcinoma. *Oncogene* 2009; **28:** 2513–2523.
31. Wu Q, Yang L, Liu H, *et al*. Elevated expression of N-acetylgalactosaminyltransferase 10 predicts poor survival and early relapse of patients with clear-cell renal cell carcinoma. *Ann Surg Oncol* 2015; **22:** 2446–2453.
32. Nilsson H, Lindgren D, Axelson H, *et al*. Features of increased malignancy in eosinophilic clear cell renal cell carcinoma. *J Pathol* 2020; **252:** 384–397.
33. Peña-Llopis S, Vega-Rubín-de-Celis S, Liao A, *et al*. BAP1 loss defines a new class of renal cell carcinoma. *Nat Genet* 2012; **44:** 751–759.
34. Stafford HS, Saltzstein SL, Shimasaki S, *et al*. Racial/ethnic and gender disparities in renal cell carcinoma incidence and survival. *J Urol* 2008; **179:** 1704–1708.
35. Capitanio U, Bensalah K, Bex A, *et al*. Epidemiology of renal cell carcinoma. *Eur Urol* 2019; **75:** 74–84.
36. Ball MW, Gorin MA, Harris KT, *et al*. Extent of renal vein invasion influences prognosis in patients with renal cell carcinoma. *BJU Int* 2016; **118:** 112–117.
37. Boström AK, Möller C, Nilsson E, *et al*. Sarcomatoid conversion of clear cell renal cell carcinoma in relation to epithelial-to-mesenchymal transition. *Hum Pathol* 2012; **43:** 708–719.
38. Minervini A, Di Cristofano C, Gacci M, *et al*. Prognostic role of histological necrosis for nonmetastatic clear cell renal cell carcinoma: correlation with pathological features and molecular markers. *J Urol* 2008; **180:** 1284–1289.
39. Miao D, Margolis CA, Gao W, *et al*. Genomic correlates of response to immune checkpoint therapies in clear cell renal cell carcinoma. *Science* 2018; **359:** 801–806.
40. Braun DA, Ishii Y, Walsh AM, *et al*. Clinical validation of PBRM1 alterations as a marker of immune checkpoint inhibitor response in renal cell carcinoma. *JAMA Oncol* 2019; **5:** 1631–1633.
41. McDermott DF, Huseni MA, Atkins MB, *et al*. Clinical activity and molecular correlates of response to atezolizumab alone or in combination with bevacizumab versus sunitinib in renal cell carcinoma. *Nat Med* 2018; **24:** 749–757.
42. Motzer RJ, Banchereau R, Hamidi H, *et al*. Molecular subsets in renal cancer determine outcome to checkpoint and angiogenesis blockade. *Cancer Cell* 2020; **38:** 803–817.e4.
43. Bakouny Z, Braun DA, Shukla SA, *et al*. Integrative molecular characterization of sarcomatoid and rhabdoid renal cell carcinoma. *Nat Commun* 2021; **12:** 808.

SUPPLEMENTARY MATERIAL ONLINE

Figure S1. Representative images of clear cell renal cell carcinomas; and tissue sampling of lesions from primary/renal vein invasion/relapsed tumours

Figure S2. Flow chart for IHC antibody selection in the present study

Figure S3. Concordance indices of ClearCode34 and immunohistology (IHC)/histology-based classification

Figure S4. Association of p53 and BAP1 expression with oncological outcomes and concordance indices of these markers in the discovery cohort

Figure S5. Relative mRNA levels of *PBRM1*, *BAP1*, and *SETD2* evaluated using a NanoString assay and tissues of the discovery cohort

Table S1. Summary of primary antibodies used and evaluation by IHC

Table S2. Association between ClearCode34 molecular subtype and clinical factors in the discovery cohort

Table S3. Factors associated with ClearCode34 model for predicting relapse in the discovery cohort

Table S4. Association between ClearCode34 molecular subtype and pathological features in the discovery cohort

Table S5. Association between the pathology-based molecular subtype and pathological features in the discovery and validation cohorts